LETTER

doi:10.1038/nature11067

All-solid-state dye-sensitized solar cells with high efficiency

In Chung[1], Byunghong Lee[2], Jiaqing He[1], Robert P. H. Chang[2] & Mercouri G. Kanatzidis[1]

Dye-sensitized solar cells based on titanium dioxide (TiO_2) are promising low-cost alternatives to conventional solid-state photovoltaic devices based on materials such as Si, CdTe and $CuIn_{1-x}Ga_xSe_2$ (refs 1, 2). Despite offering relatively high conversion efficiencies for solar energy, typical dye-sensitized solar cells suffer from durability problems that result from their use of organic liquid electrolytes containing the iodide/tri-iodide redox couple, which causes serious problems such as electrode corrosion and electrolyte leakage[3]. Replacements for iodine-based liquid electrolytes have been extensively studied, but the efficiencies of the resulting devices remain low[3–9]. Here we show that the solution-processable p-type direct bandgap semiconductor $CsSnI_3$ can be used for hole conduction in lieu of a liquid electrolyte. The resulting solid-state dye-sensitized solar cells consist of $CsSnI_{2.95}F_{0.05}$ doped with SnF_2, nanoporous TiO_2 and the dye N719, and show conversion efficiencies of up to 10.2 per cent (8.51 per cent with a mask). With a bandgap of 1.3 electronvolts, $CsSnI_3$ enhances visible light absorption on the red side of the spectrum to outperform the typical dye-sensitized solar cells in this spectral region.

Photovoltaics is a promising renewable energy technology that converts sunlight to electricity, with broad potential to contribute significantly to solving the future energy problem that humanity faces. To date, semiconductor solar cells dominate commercial markets, with crystalline Si having an 80% share; the remaining 20% is mostly thin-film solar technology, such as CdTe and $CuIn_{1-x}Ga_xSe_2$ (ref. 10). The former is an indirect bandgap semiconductor typically requiring a 300-μm-thick absorption layer, and material and processing costs are very high. The latter contains elements that are toxic and of low abundance in the Earth. However $CuIn_{1-x}Ga_xSe_2$ forms the best performing thin-film solar devices, exhibiting an efficiency of ~20%, but is more than 1.4 times as expensive as CdTe and amorphous Si. A low-cost and environmentally friendly alternative to these solid-state devices is the dye-sensitized solar cell (DSC)[1,2]. It is inexpensive to prepare, and the light-weight thin-film structures are compatible with automated manufacturing.

Conventional DSCs (Grätzel cells) consist of a self-assembled monolayer of molecular dye at the interface between a mesoporous wide-bandgap semiconductor oxide and a liquid electrolyte[1,2]. The most commonly used redox couple is iodide/tri-iodide (I^-/I^{3-}) in an organic liquid electrolyte—however, it is highly corrosive, volatile and photoreactive, interacting with common metallic components and sealing materials. Consequently, it adversely affects long-term performance and durability[3]. Alternative liquid electrolytes free of the I^-/I^{3-} redox couple have been a long-term goal in this field[5,6,11]. The ultimate solutions would be purely solid-state cells, given the inevitable problems of any liquid electrolyte, such as leakage, heavy weight and complex chemistry. Efforts have focused on using solid-state organic or p-type conducting polymer hole-transport materials (HTMs), but their conversion efficiency remains modest. Solar cells using spiro-OMeTAD (refs 9, 12) and bis-EDOT (ref. 7) exhibit the highest conversion efficiencies among organic and conducting polymer materials of 6.08% and 6.1%, respectively. (TAD is 2,2′,7,7′-tetranis(*N*,*N*-di-p-methoxyphenyl-amine)9,9′-spirobifluorene, and EDOT is 2,2′-bis(3,4-ethylenedioxythiophene).) A general problem of solid HTMs in DSCs is poor filling of the nanoporous TiO_2 layer; this interrupts the hole-conducting path between the HTM and the dye molecule adsorbed on TiO_2 (ref. 1). Despite many anticipated advantages, inorganic HTMs are uncommon. CuI, CuSCN and NiO are examples, but their mobilities are very low. The efficiency of CuI-based DSCs was found to initially reach about 3%, but rapidly photodegraded[1]. Cells of CuSCN (ref. 13) and p-type NiO particles[14] showed low efficiencies.

Here we report a new type of all-solid-state, inorganic solar cell system that consists of the p-type direct bandgap semiconductor $CsSnI_3$ and n-type nanoporous TiO_2 with the dye N719 (*cis*-diisothiocyanato-bis(2,2′-bipyridyl-4,4′-dicaboxylato) ruthenium(II) bis-(tetrabutylammonium)). We show that $CsSnI_3$ is well fitted for this purpose because of its energy gap of 1.3 eV and a remarkably high hole mobility of $\mu_h = 585\ cm^2\ V^{-1}\ s^{-1}$ at room temperature. We found that $CsSnI_3$ is soluble in polar organic solvents, such as acetonitrile, *N*,*N*,-dimethylformamide and methoxyacetonitrile. Consequently, it is solution-processable and can be transferred into TiO_2 pores at a molecular level to make intimate contacts with dye molecules and TiO_2. We present results showing that doping of $CsSnI_3$ with F and

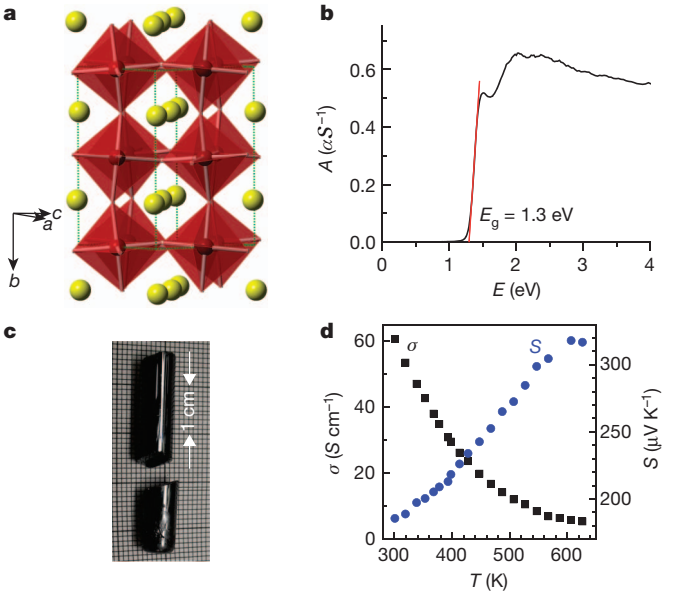

Figure 1 | Crystal structure and optical and electrical transport properties of $CsSnI_3$. **a**, Distorted three-dimensional perovskite structure of $CsSnI_3$ at room temperature. Red polyhedron, $[SnI_{6/2}]^-$; yellow sphere, Cs. **b**, Sharp absorption edge at 1.3 eV of $CsSnI_3$. *A*, absorption in units of $\alpha\,\mathcal{S}^{-1}$, where α is the absorption coefficient and $\mathcal{S}$ the scattering coefficient. *E*, energy in eV. E_g, the value of the energy gap. **c**, A typical ingot of $CsSnI_3$ grown in a Bridgman furnace. **d**, Temperature dependence of electrical conductivity (σ, filled squares) and Seebeck coefficient (*S*, filled circles).

[1]Department of Chemistry, Northwestern University, Evanston, Illinois 60208, USA. [2]Materials Science and Engineering, Northwestern University, Evanston, Illinois 60208 USA.

SnF_2 dramatically improves the photocurrent density (J_{SC}) and power conversion efficiency (η). At an optimum molar concentration of 5% F and 5% SnF_2, the cell exhibits the highest efficiency so far reported for a solid-state solar cell equipped with a dye-sensitizer: $\eta = 10.2\%$ under the standard air mass 1.5 (AM 1.5) irradiation (100 mW cm^{-2}), and $\eta = 8.51\%$ with a mask. The observed value is close to that of the highest reported performance N719-dye-containing Grätzel cell ($\eta \approx 11\%$)[15].

In our cells, $CsSnI_3$ replaces the entire liquid electrolyte. Optical absorption spectroscopy and incident photon-to-current conversion efficiency (IPCE) measurements show that our cells exhibit a red-shifted absorption edge (at 789 nm) compared to that of the typical Grätzel cell and outperform it in the red and infrared spectral regions. We note that poor performance of DSCs in this spectral range has been one of their main drawbacks.

$CsSnI_3$ adopts a distorted three-dimensional perovskite structure that crystallizes in the orthorhombic *Pnma* space group at room temperature (Fig. 1a)[16]. The compound is a direct bandgap semiconductor with a sharp optical absorption edge at 1.3 eV (Fig. 1b). Hall effect measurements on a $CsSnI_3$ thin film showed p-type conduction behaviour and a very high hole mobility of $\mu_h = 585\ cm^2\ V^{-1}\ s^{-1}$ at room temperature. To confirm this, we prepared large, bubble-free and crack-free polycrystalline ingots (Fig. 1c), and examined the electrical properties of the ingot. Thermoelectric power measurements gave positive Seebeck coefficients over the entire temperature range with linear dependence on temperature, suggesting p-type conduction (Fig. 1d). These hole mobilities are two to three orders of magnitude larger than those of any organic polymer HTM.

A schematic diagram of the relative energy levels of $CsSnI_3$, TiO_2 and the N719 dye is shown in Fig. 2. The positions of the valence band maximum (VBM) and the conduction band minimum (CBM) of $CsSnI_3$ were determined by the work function (4.92 eV) according to ultraviolet photoemission spectroscopy and the energy gap (1.3 eV). The energy levels of TiO_2 and the N719 dye are taken from the literature[5,17]. The diagram validates the excellent fit of $CsSnI_3$ in our new solid-state solar cell system, giving perfect charge separation and replacing liquid electrolytes. The CBM lies nearly in the same energy level as the lowest unoccupied molecular orbital (LUMO) of the N719 dye and above the CBM of TiO_2. The VBM lies much higher than the highest occupied molecular orbital (HOMO) of the dye. From a conventional view of DSCs, electrons generated by the dye are transported to n-type semiconductor TiO_2 and the oxidized dye is readily regenerated by p-type semiconductor $CsSnI_3$ because it is a fast hole transporter.

The cells we report here are likely to operate by a mechanism that is different from that of conventional DSCs incorporating liquid electrolyte. For example, solid-state cells made with $CsSnI_{3-x}F_x$ and TiO_2 without the dye worked as a photovoltaic devices but with a low efficiency, ~0.2% (Supplementary Information). This demonstrates that $CsSnI_{3-x}F_x$ can act as its own dye and photogenerated holes and electrons can be separated, but it is not very efficient by itself. So, if in our dye-containing cells $CsSnI_3$ absorbs the light instead of the dye, electrons and holes would be generated therein. Electrons would then be transferred to the CBM of TiO_2. At this stage, the N719 dye could act a conduit for fast charge transfer from $CsSnI_3$ facilitating rapid charge separation through hole transfer to $CsSnI_3$, resulting in high efficiency. Therefore, we presume that dye as well as $CsSnI_3$ may take part in light absorption and sensitization in a concerted way, providing a synergic effect. This issue will be the focus of our future studies.

The facile and inexpensive fabrication procedure of our cells is simple compared to other reported methods for photovoltaic devices. Powdered $CsSnI_3$ (about 100−300 mg) was dissolved in polar organic solvents (1.5 ml) to give transparent yellow solutions at room temperature. The solutions were injected onto the nanoporous TiO_2 electrode by a micropipette and dried under nitrogen. Complete evaporation of the solvent was confirmed with infrared spectroscopy. The unique advantage of $CsSnI_3$ is that a solution phase of this semiconductor material can thereby diffuse into the nanopores of TiO_2 and be stabilized as a solid phase on solvent removal. There are no by-products. Accordingly, neither high-temperature, complex chemical reactions nor high-vacuum deposition processes are required, contrary to most conventional semiconductor solar cells.

Cross-sectional scanning electron microscopy (SEM) images of our cells reveal that $CsSnI_3$ homogeneously permeates deep into the nanoporous TiO_2 substrate (Fig. 3a, b). The elemental mapping on the

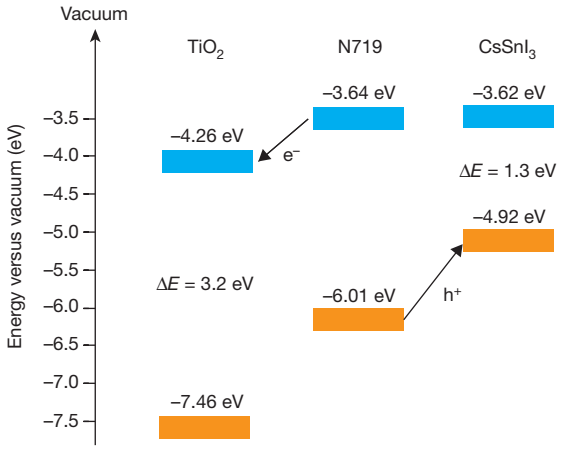

Figure 2 | Energy levels of the components of the $CsSnI_3$ solid-state solar cell. The valence band maximum (VBM; orange colour) and the conduction band minimum (CBM; blue colour) of TiO_2 and $CsSnI_3$ are represented in eV, along with the energy difference between the edges. The ground (HOMO; orange) and excited states (LUMO; blue) of N719 dye is also shown. The energy scale is referenced to the vacuum level. ΔE, e^- and h^+ represent the value of the energy gap, electron and hole, respectively.

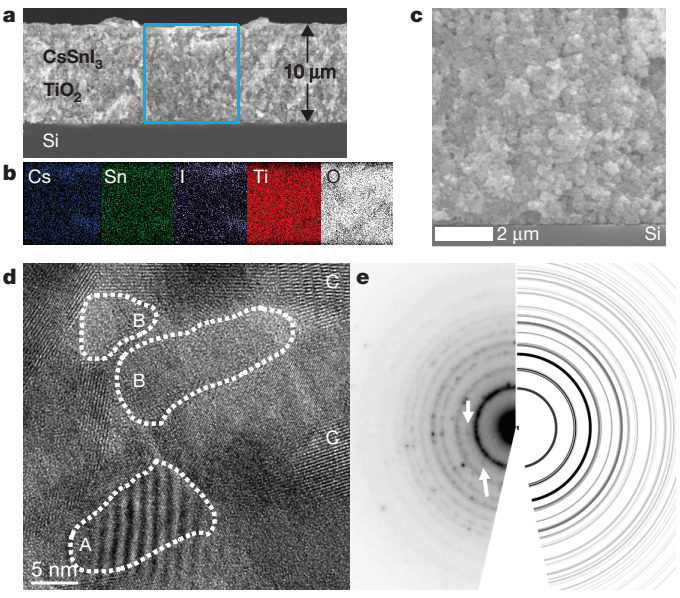

Figure 3 | Cross-sectional electron microscopy image of a $CsSnI_3/TiO_2$ cell on Si. **a**, Cross-sectional SEM image. Thickness is ~10 μm. **b**, Elemental mapping by energy dispersive spectroscopy for the rectangular area indicated by a blue box in **a**, showing homogeneous infiltration of $CsSnI_3$ into nanoporous TiO_2. **c**, Back-scattering cross-sectional SEM image, showing no discernible contrast difference. **d**, Cross-sectional HRTEM image taken near the bottom of the cell. A, $CsSnI_3$ and TiO_2 overlapped; B, high (*hkl*) index area showing unclear lattice fringes; C, TiO_2. **e**, Left panel, experimental electron diffraction pattern, indicating TiO_2 (ring patterns) and $CsSnI_3$ (spots indicated by white arrows between ring patterns); right panel, theoretical calculation of anatase TiO_2.

rectangular area shown in Fig. 3a demonstrates excellent distribution of Cs, Sn and I atoms throughout the 10-μm-thick nanoporous TiO_2 (Fig. 3b). The cross-sectional back-scattering electron image shows no discernible contrast difference over the examined area, suggesting that $CsSnI_3$ homogeneously spreads over the entire TiO_2 area (Fig. 3c). The cross-sectional high-resolution transmission electron microscopy (HRTEM) image taken at the bottom part of the TiO_2 electrode indicates that $CsSnI_3$ effectively fills the TiO_2 pores, and crystallizes on the surface of the TiO_2 (Fig. 3d). The $CsSnI_3$ and TiO_2 phases are observed to overlap with each other, as shown in area A in Fig. 3d. Area B has too high a (*hkl*) index to give clear lattice fringes. Area C in Fig. 3d indicates TiO_2. Figure 3e shows experimental electron diffraction patterns (left) in comparison with that of the theoretical TiO_2 (right). The ring patterns are assigned to anatase TiO_2, and the spots (indicated by the white arrows) between the rings of TiO_2 correspond to $CsSnI_3$.

To efficiently operate DSCs, the dye sensitizer that is adsorbed on the surface of the nanoporous TiO_2 transfers an electron to TiO_2 and is then regenerated by an electrolyte or p-type conductor[1,2]. Consequently, intimate contact between the latter and dye sensitizer is essential for perfect charge separation. However, homogeneous infiltration of p-type solid HTMs throughout the n-type nanoporous materials is the main challenge for solid-state DSCs[1,3]. Organic polymer HTMs do not efficiently infiltrate the micrometre-thick nanoporous TiO_2, degrading performance. When monomers are used for better penetration into the pores, undesirable complex chemical reactions, such as photoelectrochemical polymerization, are required[2,10]. The key characteristics of $CsSnI_3$ in our solar cells is that (1) it is solution-processable, and thus permeates throughout the entire TiO_2 structure, allowing facile charge separation and hole removal, and (2) it exhibits very large hole mobilities.

To compare the optical response of the $CsSnI_{2.95}F_{0.05}$ cell with that of a conventional Grätzel cell, the latter was prepared with N719 dye and showed ~10% efficiency[18]. The optical absorption spectrum of the $CsSnI_{2.95}F_{0.05}$-containing cell, obtained in transmission mode, reveals a well-defined edge at 789 nm, which is significantly red-shifted from that of the Grätzel cell[18] with N719 dye, at 667 nm (Fig. 4a). This observation indicates that our cell absorbs red and near-infrared light more efficiently than the Grätzel cell. Note that lack of sunlight absorption in the red and near-infrared regions has been a challenge for typical ruthenium-based dyes. Figure 4b compares the incident photon-to-current conversion efficiency (IPCE) as a function of excitation wavelength for the $CsSnI_{2.95}F_{0.05}$ cell with the Grätzel cell. The IPCE spectrum is a measure of the light response of photovoltaic devices, which is directly related to the short-circuit current. In the 550−670 nm spectral range, our cell produces a higher and broader photocurrent density in the external circuit under monochromatic illumination (per photon flux). Note that the upper limit of our IPCE measurement setting is 700 nm, resulting in a sharp drop beyond 670 nm.

The pristine $CsSnI_3$ cell gave very good photocurrent density–voltage (*J*–*V*) characteristics—open-circuit voltage (V_{OC}), fill factor (FF), short circuit current density (J_{SC}) and overall power conversion efficiency (η)—as a solid-state solar cell: $V_{OC} = 0.638$ V, FF = 66.1%, $J_{SC} = 8.82$ mA cm^{-2}, $\eta = 3.72\%$ ($\eta = V_{OC} \times J_{SC} \times FF$) (Fig. 5). To improve *J*–*V* characteristics, we studied the effect of fluorine doping on $CsSnI_3$. The optimum molar concentration of 5% fluorine doping gave a remarkable increase in J_{SC}, which reached 12.2 mA cm^{-2}, resulting in a 1.5-fold larger value of η, 5.62%. Further improvement was obtained by introducing SnF_2 into $CsSnI_{2.95}F_{0.05}$. The SnF_2 doping process was simple. The desired amounts of SnF_2 and $CsSnI_{2.95}F_{0.05}$ powders were added to polar organic solvents with stirring. The resulting solutions were injected onto the nanoporous TiO_2 electrodes. The $CsSnI_{2.95}F_{0.05}$ sample doped with 2% SnF_2 provided a 29% and 21% increase in J_{SC} (15.7 mA cm^{-2}) and η (6.81%), respectively, compared to the $CsSnI_{2.95}F_{0.05}$ sample. The optimum molar concentration of SnF_2 doping in $CsSnI_{2.95}F_{0.05}$ was found to be 5%. For the corresponding cell, the TiO_2 nanoporous film was pre-treated by a fluorine plasma etching process to increase the size of the nanopores and nanochannels as described in the literature[18]. This also possibly helps to reduce surface states and charged particle recombination[18]. The resulting cell showed very good *J*–*V* characteristics: $J_{SC} = 17.4$ mA cm^{-2}; $V_{OC} = 0.730$ V; FF = 72.9%, $\eta = 9.28\%$.

To fully employ the photon flux absorbed, we applied two layers of the three-dimensional inverse photonic crystal ZnO (ref. 19) over the counter electrode of the same cell. Each layer of the photonic crystal had a different hole diameter—values of 375 nm and 410 nm were used. The corresponding cell exhibited $J_{SC} = 19.2$ mA cm^{-2}, $V_{OC} = 0.732$ V, FF = 72.7% and $\eta = 10.2\%$. When a mask was applied on the cell, $\eta = 8.51\%$ was observed (Supplementary Information). The observed efficiency is the highest among any kind of dye-sensitized solar cell free of liquid electrolyte, and is close to that of

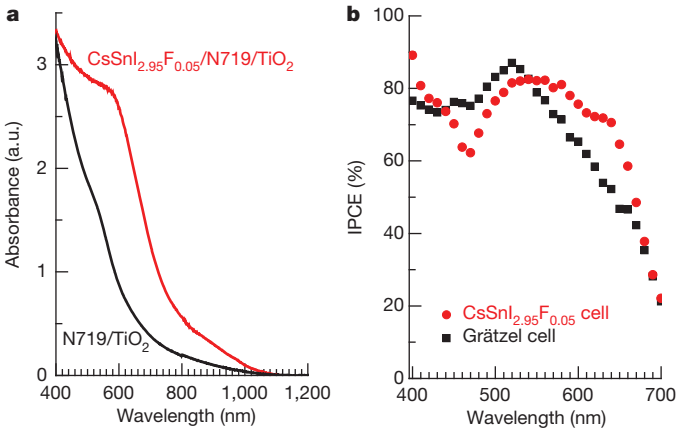

Figure 4 | Optical response of the $CsSnI_{2.95}F_{0.05}$ cell and a conventional Grätzel cell. **a**, Optical absorbance spectra of the devices consisting of $CsSnI_{2.95}F_{0.05}$/N719 dye/TiO_2 (red line) and N719 dye/TiO_2 (liquid electrolyte was not added here) (black line). **b**, The IPCE spectrum as a function of the wavelength of monochromatic light that impinges on the $CsSnI_{2.95}F_{0.05}$ cell (filled circles) in comparison with that of the N719-dye-containing Grätzel cell (filled squares).

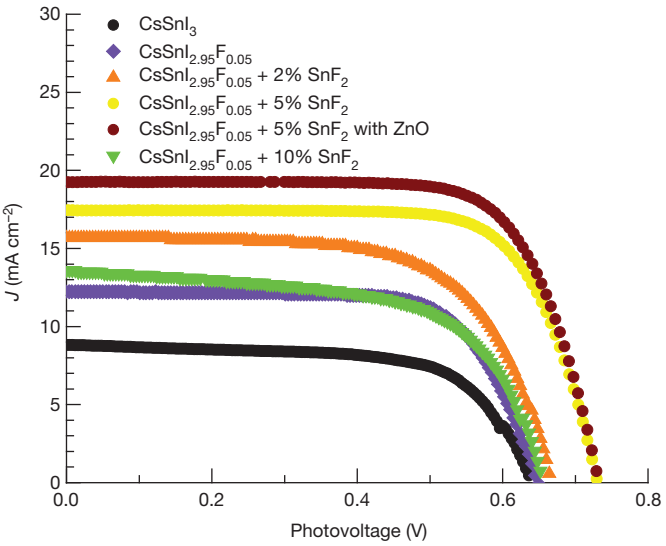

Figure 5 | Photocurrent density–voltage (*J*–*V*) characteristics of the solar cell devices under irradiation of 100 mW cm^{-2} simulated AM 1.5 sunlight. These solar cells incorporated $CsSnI_3$ and $CsSnI_{2.95}F_{0.05}$ doped with SnF_2. Fluorine and SnF_2 doping increase photocurrent density, resulting in an improved power conversion efficiency (η). Application of three-dimensional ZnO photonic crystal layers further enhances the photocurrent density, and gives the highest value of η (10.2%) for the cell of $CsSnI_{2.95}F_{0.05}$ doped with SnF_2.

the high performance Grätzel cell ($\eta \approx 11\%$). The samples with 10% SnF_2 resulted in a reduction in J_{SC} (measured value, 13.6 mA cm^{-2}) and η (measured value, 5.46%). Compounds of the type $CH_3NH_3PbX_3$ (X = Br, I), which are isostructural with $CsSnI_3$, have been used as visible light sensitizers adsorbed on the TiO_2 surface for photovoltaic cells. These cells, however, employed organic liquid electrolyte containing LiX/X_2 redox couples, and exhibited low efficiency[20].

We have demonstrated the superior performance of the p-type inorganic high-hole-mobility semiconductor $CsSnI_{3-x}F_x$ and its ability to replace the problematic organic liquid electrolytes in dye-sensitized solar cells (DSCs). We refer to these solid-state solar cells as solid-state DSCs (SSDSCs). Unlike liquid electrolytes with their complex chemistry, crystalline inorganic solids promise long-term stability, and also enable theoretical calculations based on electronic structure and further improvement of their photovoltaic properties. The new solar cells described here are all-solid-state, inorganic systems. The $CsSnI_{3-x}F_x$ compounds consist of inexpensive, abundant elements and are solution-processable at room temperature, allowing for low-cost processing. Our new cell reaches a conversion efficiency of ~10.2% (8.51% with a mask), and is the first example of an all solid-state dye-sensitized solar cell system that may eventually exceed the performance of a liquid electrolyte Grätzel cell. With further optimization and new dyes[11], much higher efficiencies are likely. This work opens up the possibility of semiconducting solid materials becoming 'state of the art' and promoting much higher efficiencies than have been possible with conventional DSCs.

METHODS SUMMARY

Synthesis of $CsSnI_{3-x}F_x$. Pure $CsSnI_{3-x}F_x$ ($0 \leq x \leq 1$) compounds were achieved by heating a stoichiometric mixture of CsI, SnI_2 and SnF_2 in an evacuated Pyrex or fused silica tube at 450 °C for 30 min, followed by quenching to room temperature. The ground powders (~100–350 mg) were dissolved/dispersed in anhydrous polar organic solvents (1.5 ml): *N*,*N*-dimethylformamide, acetonitrile and methoxyacetonitrile. For SnF_2 doping, appropriate ratios of $CsSnI_{2.95}F_{0.05}$ and SnF_2 powders were stirred in the same organic solvents.

TiO_2 electrode preparation and device assembly. TiO_2 electrode preparation, a fluorine plasma etching process, and device assembly are described in the literature[18]. The solutions of $CsSnI_{3-x}F_x$ (with SnF_2 if necessary) were injected into the cell by a micropipette and dried. The ZnO photonic crystals were prepared as described in the literature[19]. They were attached on the top of the counter-electrode if necessary.

Full Methods and any associated references are available in the online version of the paper at www.nature.com/nature.

Received 6 February; accepted 8 March 2012.

1. Hagfeldt, A., Boschloo, G., Sun, L. C., Kloo, L. & Pettersson, H. Dye-sensitized solar cells. *Chem. Rev.* **110,** 6595–6663 (2010).
2. Grätzel, M. Recent advances in sensitized mesoscopic solar cells. *Acc. Chem. Res.* **42,** 1788–1798 (2009).
3. Yanagida, S., Yu, Y. H. & Manseki, K. Iodine/iodide-free dye-sensitized solar cells. *Acc. Chem. Res.* **42,** 1827–1838 (2009).
4. Koh, J. K., Kim, J., Kim, B., Kim, J. H. & Kim, E. Highly efficient, iodine-free dye-sensitized solar cells with solid-state synthesis of conducting polymers. *Adv. Mater.* **23,** 1641–1646 (2011).
5. Daeneke, T. *et al.* High-efficiency dye-sensitized solar cells with ferrocene-based electrolytes. *Nature Chem.* **3,** 211–215 (2011).
6. Wang, M. K. *et al.* An organic redox electrolyte to rival triiodide/iodide in dye-sensitized solar cells. *Nature Chem.* **2,** 385–389 (2010).
7. Liu, X. Z. *et al.* An efficient organic-dye-sensitized solar cell with in situ polymerized poly(3,4-ethylenedioxythiophene) as a hole-transporting material. *Adv. Mater.* **22,** E150–E155 (2010).
8. Jiang, K. J. *et al.* Photovoltaics based on hybridization of effective dye-sensitized titanium oxide and hole-conductive polymer P3HT. *Adv. Funct. Mater.* **19,** 2481–2485 (2009).
9. Bach, U. *et al.* Solid-state dye-sensitized mesoporous TiO_2 solar cells with high photon-to-electron conversion efficiencies. *Nature* **395,** 583–585 (1998).
10. Bisquert, J. Dilemmas of dye-sensitized solar cells. *ChemPhysChem* **12,** 1633–1636 (2011).
11. Yella, A. *et al.* Porphyrin-sensitized solar cells with cobalt (II/III)-based redox electrolyte exceed 12 percent efficiency. *Science* **334,** 629–634 (2011).
12. Cai, N. *et al.* An organic D-π-A dye for record efficiency solid-state sensitized heterojunction solar cells. *Nano Lett.* **11,** 1452–1456 (2011).
13. O'Regan, B., Lenzmann, F., Muis, R. & Wienke, J. A solid-state dye-sensitized solar cell fabricated with pressure-treated P25-TiO_2 and CuSCN: analysis of pore filling and IV characteristics. *Chem. Mater.* **14,** 5023–5029 (2002).
14. Bandara, J. & Weerasinghe, H. Solid-state dye-sensitized solar cell with p-type NiO as a hole collector. *Sol. Energy Mater. Sol. Cells* **85,** 385–390 (2005).
15. Kroon, J. M. *et al.* Nanocrystalline dye-sensitized solar cells having maximum performance. *Prog. Photovolt. Res. Appl.* **15,** 1–18 (2007).
16. Shum, K. *et al.* Synthesis and characterization of $CsSnI_3$ thin films. *Appl. Phys. Lett.* **96,** 221903 (2010).
17. Grätzel, M. Photoelectrochemical cells. *Nature* **414,** 338–344 (2001).
18. Lee, B., Buchholz, D. B., Guo, P. J., Hwang, D. K. & Chang, R. P. H. Optimizing the performance of a plastic dye-sensitized solar cell. *J. Phys. Chem. C* **115,** 9787–9796 (2011).
19. Lee, B. *et al.* Materials, interfaces, and photon confinement in dye-sensitized solar cells. *J. Phys. Chem. B* **114,** 14582–14591 (2010).
20. Kojima, A., Teshima, K., Shirai, Y. & Miyasaka, T. Organometal halide perovskites as visible-light sensitizers for photovoltaic cells. *J. Am. Chem. Soc.* **131,** 6050–6051 (2009).

Supplementary Information is linked to the online version of the paper at www.nature.com/nature.

Acknowledgements The authors acknowledge support for this collaborative research: NSF-DMR 0843962 for R.P.H.C.; DOE Energy Frontier Research Center, ANSER, DE-SC0001059 for B.H.L., J.H. and M.G.K.; the Initiative for Energy and Sustainability at Northwestern (ISEN) for I.C. Device testing and measurements were done in the ANSER Facilities and materials characterization was performed in the NSFMRSEC Facilities (DMR-1121262).

Author Contributions I.C. and M.G.K. conceived and designed the experiments and prepared the manuscript. I.C. synthesized materials. R.P.H.C. and B.L. designed and fabricated the solar cells, I.C. and B.L. performed measurements. J.H. collected TEM data. I.C., B.L., R.P.H.C. and M.G.K. discussed the results and wrote the manuscript.

Author Information Reprints and permissions information is available at www.nature.com/reprints. The authors declare no competing financial interests. Readers are welcome to comment on the online version of this article at www.nature.com/nature. Correspondence and requests for materials should be addressed to M.G.K. (m-kanatzidis@northwestern.edu).

METHODS

TiO_2 electrode preparation. High-purity anatase TiO_2 nanoparticles and their paste form were prepared as described in the literature[18]. The obtained paste was spread on the fluorine-doped SnO_2 glass substrate (FTO, Pilkington, TEC 8 glass, 8 Ω per square, 2.3 mm thick) using a doctor blade, followed by gradual calcination to remove residual polymers under an air flow at 150 °C for 15 min, at 320 °C for 10 min and at 500 °C for 30 min, giving a pure anatase TiO_2 nanoparticle film with a flat and smooth surface. A fluorine plasma etching process was applied as described in the literature if necessary[18]. The film thickness was determined by a surface profiler (Tencor P-10). The ZnO photonic crystals were prepared as described in the literature[19]. They were attached on the top of the counter-electrode if necessary.

Device assembly. The TiO_2 electrode was immersed in an ethanol solution containing purified 3×10^{-4} M (*cis*-diisothiocyanato-bis(2,2′-bipyridyl-4,4′-dicaboxylato) ruthenium(II) bis(tetrabutylammonium)) (N719, Solaronix) for 18 h at room temperature, followed by rinsing with ethanol and drying under a nitrogen flow. The counter-electrode was prepared by coating FTO glass with a thin layer of a 5 mM H_2PtCl_6 solution (in isopropanol), followed by heating at 400 °C for 20 min. The two electrodes were sealed together with thermal melt polymer film (Surlyn, DuPont). The typical active area of the cell was ~0.2–0.3 cm^2. The exact area of photoanode was calibrated by an optical scanner under a resolution of 600 dots per inch. The $CsSnI_{3-x}F_x$ without SnF_2 solutions were injected into the cell by a micropipette and dried.

Device characterization. The devices were evaluated under 100 mW cm^{-2} standard air mass 1.5 global (AM 1.5G) sunlight simulation with a class A solar cell analyser (Spectra Nova Tech.). A silicon solar cell fitted with a KG3 filter tested and certified by the National Renewable Energy Laboratory (NREL) was used for calibration. The KG3 filter accounts for the different light absorptions of the dye-sensitized solar cell and silicon, and ensures that the spectral mismatch correction factor approaches unity. Incident photon-to-current conversion efficiency was measured using a monochromator (Jobin-Yvon fluorescence spectrometer) and a potentiostat (CH Instruments 1202). Electrochemical impedance spectroscopy was performed under the same light illumination with an impedance analyser (Solartron 1260) and a potentiostat (Solartron 1287) when the device was tested at its V_{OC}. An additional low amplitude modulation sinusoidal voltage of 10 mV_{rms} was also applied between the anode and cathode of the device over the frequency range of 0.05−150 kHz.

Electron microscopy. SEM images were taken with a Hitachi S-4800II SEM. TEM investigations were carried out in a JEOL 2100F microscope operating at 200 keV accelerating voltage.

$CsSnI_3$ characterization. Hall effect measurement. The $CsSnI_3$ sample was subjected to a flow of nitrogen gas to protect it from oxidation during measurements. A d.c. current source (6220 Keithley Instruments) was used to supply a constant 100 mA current through the sample while an external magnetic field up to ±1.4 T was applied in steps of 0.25 T. The voltage response, both in the positive and negative directions of the magnetic field, was recorded at each respective step by a nanovoltmeter (2182A Keithley Instruments) and the half-difference of the two signals was recorded as the Hall voltage.

Charge-transport properties. The ingot was cut and polished into a rectangular shape with dimensions of ~2 mm × 3 mm × 8 mm under N_2 atmosphere. Electrical conductivity and Seebeck coefficient were measured simultaneously under He atmosphere from room temperature to 650 K on a ULVAC-RIKO ZEM-3 instrument system. The mechanical electrodes made of Rh/Pt and Pt were directly contacted to the ingot with no use of a chemical paste.

Optical absorption spectroscopy. Optical diffuse reflectance measurements were performed at room temperature using a Shimadzu UV-3101 PC spectrometer operating in the 200–2,500 nm region. The reflectance versus wavelength data generated were used to estimate the bandgap of the material by converting reflectance to absorption data according to the Kubelka-Munk equation: $\alpha/S = (1-R)^2\,(2R)^{-1}$, where R is the reflectance and α and S are the absorption and scattering coefficients, respectively.